

1
2
3
4
5
6
7
8
9
10
11
12
13
14
15
16
17
18
19
20
21
22
23
24
25
26
27
28
29
30
31
32
33
34
35
36
37
38
39
40
41
42
43
44
45
46
47
48
49
50
51
52
53
54
55
56
57
58
59
60
61
62
63
64
65

Parameter Estimation of an Electrochemistry-based Lithium-ion Battery Model using a Two-Step Procedure and a Parameter Sensitivity Analysis

N. Jin, D.L. Danilov*, P.M.J. Van den Hof, M.C.F. Donkers
Control Systems Group, Department of Electrical Engineering
Eindhoven University of Technology, Den Dolech 2, 5600MB Eindhoven
* Corresponding author. Email: d.danilov@tue.nl, phone: +31402473113.

Abstract

Lithium-ion batteries are indispensable in various applications owing to their high specific energy and long service life. Lithium-ion battery models are used for investigating the behavior of the battery and enabling power control in applications. The Doyle-Fuller-Newman (DFN) model is a popular electrochemistry-based model, which characterizes the dynamics in the battery through diffusions in solid and electrolyte, and predicts current/voltage response. However, the DFN model contains a large number of parameters that need to be estimated in order to obtain an accurate battery model. In this paper, a computationally feasible noninvasive two-step estimation approach is proposed that only uses voltage and current measurements of the battery under consideration. In the two-step procedure, the parameters are divided into two groups. The first group contains thermodynamic parameters, which are estimated using low-current discharges, while the second group contains kinetic parameters, which are estimated using a well-designed highly-dynamic pulse (dis-)charge current. A parameter sensitivity analysis is done to find a subset of parameters that can be reliably estimated using current and voltage measurements only. Experimental data are collected for 12 Ah Nickel Cobalt Aluminum pouch Lithium-ion cell. The voltage predictions of the identified model are compared with several experimental data sets to validate the model. A Root-Mean-Square-Error (RMSE) between model predictions and experimental data smaller than 16 mV

1
2
3
4
5
6
7
8
9 is achieved.

10 *Keywords:* Lithium-ion battery, DFN model, thermodynamic, kinetic,
11 sensitivity analysis, parameter estimation
12
13

14 **1. Introduction**

15
16
17
18
19
20
21
22
23
24
25
26
27
28
29
30
31
32
33
34
35
36
37
38
39
40
41
42
43
44
45
46
47
48
49
50
51
52
53
54
55
56
57
58
59
60
61
62
63
64
65
Lithium-ion (Li-ion) batteries are known to have a high energy density and a long service life. They have been successfully used in the automotive industry, which enables the production of low-emission hybrid vehicles and zero-emission full electric vehicles [1, 2]. To facilitate the analysis, design and control of the batteries, models of Li-ion batteries are required. For instance, these models are used in typical functionalities of the Battery Management System (BMS), such as State-of-Charge (SoC) estimation, capacity fade estimation and real-time control [3, 4, 5, 6, 7]. An accurate model plays a pivotal role in investigation and proper control of the battery.

Among the available battery models, the Equivalent Circuit Model (ECM) and the Doyle-Fuller-Newman (DFN) model are popular ones. The ECM describes the input/output behavior of batteries through an electrical circuit consisting of a voltage source, a series resistance and a parallel connection of a resistor and capacitor, see, e.g., [8], while the DFN model is an electrochemistry-based model, which characterizes the dynamics in Li-ion battery based on concentrations and potentials [9, 10]. Several papers report methods for estimating the parameters of the ECM of Li-ion batteries, see, e.g., [11, 12, 13, 14, 15], papers presenting methods for estimation the parameters of the DFN model seem to be scarce.

Although some parameters of the DFN model (e.g., layer thicknesses and diffusion coefficients) can be determined with direct experiments, it is still complicated and challenging to carry out these measurements. Moreover, since the number of parameters is large and the estimation procedure is computationally complex, it is hard to estimate all parameters in the full DFN model. For this reason, parameter estimation has been mostly applied to simplified DFN

1
2
3
4
5
6
7
8
9 models, such as the single particle model [16] [17, 18, 19, 20]. Most of these
10 works relies on Gauss-Newton method for nonlinear optimization to perform
11 parameter estimation [17, 20], while some have used a homotopy optimization
12 method [18, 19]. Though parameter estimation by a Genetic algorithm had
13 been successfully used to estimate parameters in [21], only a few results are
14 available on parameter estimation of the full DFN model. In a number of
15 sources [11, 12, 13, 14, 15, 17, 18, 19, 20], various parameters are estimated but
16 the parameters choice remains unexplained.
17

18
19
20
21 In this paper, the parameter estimation of the full DFN model is considered
22 to obtain a high-fidelity battery model. A computationally feasible two-step
23 estimation approach is developed that uses only voltage and current measure-
24 ments. In the proposed two-step procedure, the original set of parameters is split
25 into two: thermodynamic parameters and kinetic parameters, which are esti-
26 mated separately. The thermodynamic parameters are related to the capacity,
27 which are estimated using low-current discharges, while the kinetic parameters
28 are estimated using highly-dynamic pulse (dis-)charge current. A parameter
29 sensitivity analysis based on QR factorization [22] is applied to find a subset of
30 parameters that can be reliably estimated, which leads to a simplified estimation
31 procedure. Additionally, an experimental input current profile is designed for es-
32 timation and all data are collected from 12 Ah Nickel Cobalt Aluminum (NCA)
33 Li-ion batteries. Giving the designed current input to the model and measur-
34 ing the experimental voltage of the battery, the DFN model is parameterized
35 through the estimation of the sensitive parameters using nonlinear least-square
36 optimization [23, 24]. The estimated model is validated by comparing the pre-
37 dictions of model to the measurements on different data sets so as to ensure the
38 model is reliable.
39

40
41
42
43
44
45
46
47
48
49
50 The remainder of this paper is organized as follows. In Section 2, the DFN
51 model is outlined and a numerical computation procedure for implementing the
52 DFN model is given. Two groups of parameters: thermodynamic and kinetic,
53 accompanied with their expected ranges and nominal values will be presented
54 in Section 3. Estimation of the thermodynamic parameters by determining the
55
56
57
58

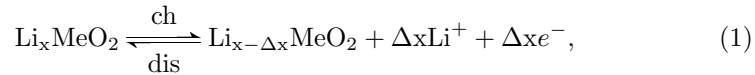
1
2
3
4
5
6
7
8
9 equilibrium voltage and the capacity of the battery will be done in Section
10 4. Section 5 deals with identifying the most sensitive subset in the group of
11 kinetic parameters using QR factorization and those parameters are estimated
12 using nonlinear least-square optimization. Finally, the model is validated using
13 different experimental data sets (constant discharge and hybrid cycle) in Section
14 6 and conclusions will be drawn in Section 7.

20 2. Model description and implementation

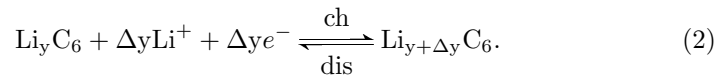
21
22 In this paper, the DFN model is considered, see, e.g., [9, 10]. This model is
23 derived according to the electrochemical description of the (dis-)charging process
24 in a Li-ion battery, which determines the dynamics of ionic concentrations and
25 potentials in the battery. In this section, the fundamental governing equations
26 and the implementation of the DFN model will be given.

30 2.1. Fundamentals of DFN model

31
32 Fig. 1 schematically outlines a Li-ion cell, showing its three main regions:
33 the negative composite electrode, the separator and the positive composite elec-
34 trode. Composite electrodes contain two phases: a liquid phase, which is elec-
35 trolyte and a solid phase which contains active material particles. The elec-
36 trolyte is a lithium salt dissolved in an organic solvent and can be considered as
37 a binary system. Electrolyte fills a liquid phase in electrodes and separator. The
38 main storage reaction at the cathode side of the Li-ion battery flows according
39 to



45 where Me represents transition metal, in line with cathode composition (e.g.
46 Me = Co for traditional chemistry, or Me = Ni_aCo_bAl_{1-a-b} for NCA cells).
47 Note that for proper (reversible) operation of Li-ion batteries, not all lithium
48 can be withdrawn from the cathode, i.e. $x \geq x_{\min}$, for value x_{\min} close to 0.5.
49 The electrochemical reaction at anode side is given by



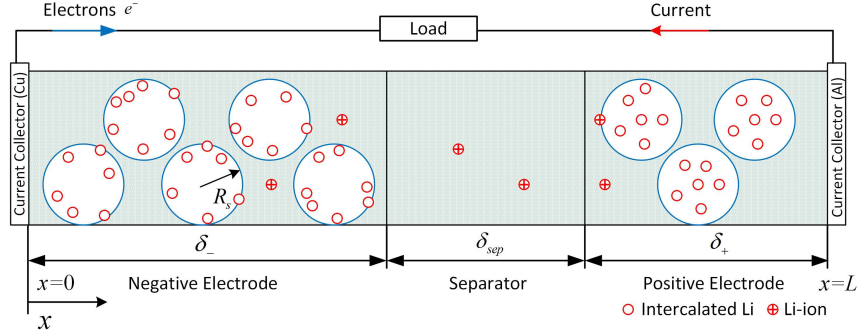


Figure 1: Schematic one-dimensional representation of a Li-ion battery.

During discharging, lithium deintercalates from the anode, enters the liquid phase and moves to the cathode through the separator. The reverse process occurs during charging. In the liquid phase, the Li-ions movement is caused by a combination of diffusion and migration across the electrolyte. Therefore, the ionic concentrations and potentials in both electrodes and electrolyte change during the operation of the battery. The DFN model characterizes these dynamics in the Li-ion battery by using the porous electrode theory and the concentrated solution theory [25]. Within the DFN model, the intertemporal response of a cell (in terms of voltage and current) can be predicted from a fundamental characterization of the physical phenomena involved in the process. In particular, thermodynamics (the equilibrium potentials of the electrodes), kinetics (the rate of the charge transfer reactions) and mass/charge transport (the movement of ions through solid and liquid media) are considered.

2.2. Governing equations

The DFN model is a pseudo 2-dimensional model and consists of a set of coupled partial differential equations, ordinary differential equations and algebraic equations. The model describes the transport of Li-ions is determined by diffusion in solid phase and in the liquid phase and charge conservation in both electrodes described by Ohm's law. A brief summary of the model's governing equations is given below.

- 1
2
3
4
5
6
7
8
9
- The concentration of Li-ions in solid phase $C_{s,k}(x, r, t)$ in the negative ($k = n$) and the positive electrode ($k = p$) depends on the particle position $x \in [0, \delta_-]$ for positive electrode and $x \in [L - \delta_+, L]$ for negative electrode, where δ_- and δ_+ are the thickness of negative and positive electrode, respectively, and the radial position within a particle $r \in [0, R_s]$, where R_s is the radius of particles, and time $t \in \mathbb{R}_+$. The ionic concentration inside a single spherical active material particle is described by Fick's law of diffusion, i.e.,

$$\frac{\partial C_{s,k}}{\partial t} = \frac{D_{s,k}}{r^2} \frac{\partial}{\partial r} \left(r^2 \frac{\partial C_{s,k}}{\partial r} \right), \quad (3a)$$

with boundary conditions

$$\left. \frac{\partial C_{s,k}}{\partial r} \right|_{r=0} = 0, \quad -D_{s,k} \left. \frac{\partial C_{s,k}}{\partial r} \right|_{r=R_s} = \frac{j_{\text{Li},k}}{a_{s,k} F}, \quad (3b)$$

where $k \in \{n, p\}$, represents negative or positive electrode. In this expression, $D_{s,k}$ are the diffusion coefficients in solid phase, $j_{\text{Li},k}$ is the volume-specific rate of the electrochemical reaction, which will be defined below, F is Faraday's constant ($96487 \text{ C}\cdot\text{mol}^{-1}$) and the specific interfacial active surface area $a_{s,k} = 3\epsilon_{s,k}/R_s$, in which $\epsilon_{s,k}$ is the volume fraction of active particles in both electrodes.

- 10
11
12
13
14
15
16
17
18
19
20
21
22
23
24
25
26
27
28
29
30
31
32
33
34
35
36
37
38
39
- The concentration of Li-ions in the liquid phase $C_e(x, t)$, where $x \in [0, L]$, is governed by Fick's law of linear diffusion combined with an intercalation current density term j_{Li} , transferring ions between the solution and the solid, i.e.,

$$\epsilon_e \frac{\partial C_e}{\partial t} = \frac{\partial}{\partial x} \left(D_e^{\text{eff}} \frac{\partial C_e}{\partial x} \right) + \frac{1 - t_+}{F} j_{\text{Li}}, \quad (4a)$$

with zero-flux boundary conditions at the current collectors

$$\left. \frac{\partial C_e}{\partial x} \right|_{x=0} = \left. \frac{\partial C_e}{\partial x} \right|_{x=L} = 0. \quad (4b)$$

40
41
42
43
44
45
46
47
48
49
50
51
52
53
54
55
56
57
58

In these expressions, ϵ_e is electrolyte phase volume fraction (porosity) and t_+ is the transference number of Li ions, D_e^{eff} denotes the effective diffusion coefficient in the electrolyte phase, which is calculated from a reference

coefficient using the Bruggeman relation, i.e., $D_e^{\text{eff}} = D_e \epsilon_e^p$, where p is Bruggeman porosity exponent, given by $p = 1.5$.

- The potentials in the solid phase $\phi_{s,k}(x, t)$ is given by

$$\frac{\partial}{\partial x} (\sigma_k^{\text{eff}} \frac{\partial \phi_{s,k}}{\partial x}) = j_{\text{Li},k}, \quad (5a)$$

with boundary conditions

$$-\sigma_n^{\text{eff}} \frac{\partial \phi_{s,n}}{\partial x} \Big|_{x=0} = \frac{I_{\text{app}}}{A}, \quad \frac{\partial \phi_{s,n}}{\partial x} \Big|_{x=\delta_-} = 0, \quad (5b)$$

$$\frac{\partial \phi_{s,p}}{\partial x} \Big|_{x=L-\delta_+} = 0, \quad -\sigma_p^{\text{eff}} \frac{\partial \phi_{s,p}}{\partial x} \Big|_{x=L} = \frac{I_{\text{app}}}{A}. \quad (5c)$$

where $k \in \{n, p\}$, denotes the negative or positive electrode. In this expression, $\sigma_k^{\text{eff}} = \sigma_k \epsilon_{s,k}$ denotes the effective electrical conductivity, in which σ_k represents the electrical conductivity in solid active material, A is the electrode plate area and $I_{\text{app}}(t)$ is the applied current, as an input of the model.

- The potential in the electrolyte phase $\phi_e(x, t)$ is described by

$$\frac{\partial}{\partial x} (\kappa^{\text{eff}} \frac{\partial \phi_e}{\partial x} + \kappa_D^{\text{eff}} \frac{\partial \ln C_e}{\partial x}) = -j_{\text{Li}}, \quad (6a)$$

with boundary conditions

$$\frac{\partial \phi_e}{\partial x} \Big|_{x=0} = \frac{\partial \phi_e}{\partial x} \Big|_{x=L} = 0. \quad (6b)$$

In above equations, $\kappa^{\text{eff}} = \kappa \epsilon_e^p$ denotes effective ionic conductivity, with $\kappa = 15.8 C_e \exp(0.85(1000 C_e)^{1.4})$. Moreover, the effective diffusional conductivity κ_D^{eff} is derived from concentrated solution theory and given by

$$\kappa_D^{\text{eff}} = \frac{2RT\kappa^{\text{eff}}}{F} (t_+ - 1) \left(1 + \frac{\partial \ln f_{\pm}}{\partial \ln C_e}\right), \quad (7)$$

where R is the universal gas constant ($8.3143 \text{ J}\cdot\text{mol}^{-1}\text{K}^{-1}$), T is the absolute temperature and f_{\pm} is the activity coefficient, which is assumed to be constant in the present work, leading to the simplified expression

$$\kappa_D^{\text{eff}} = \frac{2RT\kappa^{\text{eff}}}{F} (t_+ - 1). \quad (8)$$

The four governing equations (3)-(6) are coupled with the volume-specific rate of reaction $j_{Li,k}$, which satisfies Butler-Volmer electrochemical kinetic expression

$$j_{Li,k} = a_{s,k} i_{0,k} \left(\exp\left(\frac{\alpha_k F}{RT} \eta_k\right) - \exp\left(\frac{(\alpha_k - 1) F}{RT} \eta_k\right) \right), \quad (9)$$

where α_k is charge transfer coefficient for k -th electrode. In this expression, $i_{0,k}$ is the exchange current density given by

$$i_{0,k} = k_0 C_e^{\alpha_k} (C_{s,k}^{\max} - C_{s,k}^{\text{surf}})^{\alpha_k} (C_{s,k}^{\text{surf}})^{1-\alpha_k}, \quad (10)$$

where k_0 is a kinetic rate constant, $C_{s,k}^{\max}$ denotes the maximum concentration in the solid phase and $C_{s,k}^{\text{surf}}(x, t) = C_{s,k}(R_s, x, t)$ is the concentration at the particle surface. Moreover, η_k represents the overpotential at both electrodes, which is related to the potentials in two phases and the equilibrium potential as

$$\eta_k = \phi_{s,k} - \phi_e - U_k, \quad (11)$$

where U_k , $k \in \{p, n\}$, is the equilibrium potential in electrodes, which is always evaluated as a predefined function of the solid phase concentration at the particle surface $C_{s,k}(x, R_s, t)$, written as

$$U_p = U_p(x), \quad U_n = U_n(y), \quad (12)$$

where $x(x, t) = C_{s,p}(x, R_s, t)/C_{s,p}^{\max}$ and $y(x, t) = C_{s,n}(x, R_s, t)/C_{s,n}^{\max}$ are the normalized concentrations at the surface of the positive and negative electrodes accordingly. Finally, the terminal voltage is calculated by the difference between the solid phase potential at the two current collectors, minus an Ohmic drop due to contact resistance, given by

$$V(t) = \phi_s(L, t) - \phi_s(0, t) - \frac{R_f}{A} I_{\text{app}}(t), \quad (13)$$

where R_f denotes the contact resistance.

2.3. Model implementation

In order to obtain the predicted output of the DFN model for proper parameter estimation, a reliable numerical implementation of the model is needed. The

implementation method used in this paper is based on a numerical procedure proposed by [26]. The main idea for implementing the DFN model can be summarized into the following three steps. The first step is a spatial discretization of (3)-(6), by approximating the $\frac{\partial}{\partial x}$ term in these equations using a finite-volume or finite-difference method, leading to a set of nonlinear Differential Algebraic Equations (DAE) of the form:

$$\begin{cases} \frac{dC}{dt} = f(C, \phi, \mathbf{P}) \\ 0 = g(C, \phi, I_{\text{app}}, \mathbf{P}), \end{cases} \quad (14)$$

where C denotes the spatially discretized concentrations, ϕ denotes the spatially discretized potentials, I_{app} is the applied current and \mathbf{P} is the vector of all the model parameters. The functions f and g are nonlinear functions resulting from the spatially discretized modelling equations.

The second step in the numerical implementation is a backward Euler discretization over time, leading to:

$$\begin{cases} C(t_{n+1}) = C(t_n) + (t_{n+1} - t_n)f(C(t_{n+1}), \phi(t_{n+1}), \mathbf{P}) \\ 0 = g(C(t_{n+1}), \phi(t_{n+1}), I_{\text{app}}(t_{n+1}), \mathbf{P}), \end{cases} \quad (15)$$

which is a set of purely algebraic equations. Eqn. (15) is finally solved using an iterative numerical procedure based on Gauss-Newton's method, which represents the third step. After obtaining the solution of the dependent variables of the model (C_s, C_e, ϕ_s, ϕ_e), the cell terminal voltage $V(t)$, as the output of the DFN model can be calculated by (13). More details on the model implementation can be found in [26].

3. Parameters grouping and ranging

The DFN model contains a large number of parameters related to design, size and electrochemistry of the battery. Various physical parameters have different influence on the behavior of the battery and they can be divided into two groups: thermodynamic parameters and kinetics parameters. In this section, the two

Table 1: Thermodynamic and kinetic parameters with ranges and nominal values

Thermodynamic parameters						
m	Parameter	Dimension	Description	Nominal value	Range	Scaling
1	δ_-	μm	Negative electrode thickness	50		
2	δ_+	μm	Positive electrode thickness	36.4		
3	$\epsilon_{s,n}$		Active article volume fraction in negative electrode	0.58		
4	$\epsilon_{s,p}$		Active article volume fraction in positive electrode	0.5		
5	$C_{s,n}^{\text{max}}$	$\text{mol}\cdot\text{m}^{-3}$	Maximum solid phase concentration in negative electrode	$16.1\cdot 10^3$		
6	$C_{s,p}^{\text{max}}$	$\text{mol}\cdot\text{m}^{-3}$	Maximum solid phase concentration in positive electrode	$23.9\cdot 10^3$		
7	$y_{0\%}$		Stoichiometry at 0% state of charge in negative electrode	0.126		
8	$x_{0\%}$		Stoichiometry at 0% state of charge in positive electrode	0.936		
9	$y_{100\%}$		Stoichiometry at 100% state of charge in negative electrode	0.676		
10	$x_{100\%}$		Stoichiometry at 100% state of charge in positive electrode	0.442		
11	A	m^2	Electrode plate area	1.84		
Kinetic parameters						
1	$\epsilon_{e,n}$		Electrolyte volume fraction in negative electrode	0.21	[0, 0.42]	(17a)
2	$\epsilon_{e,\text{sep}}$		Electrolyte volume fraction in separator	0.5	[0, 1]	(17a)
3	$\epsilon_{e,p}$		Electrolyte volume fraction in positive electrode	0.25	[0, 0.48]	(17b)
4	D_e	$\text{m}^2\cdot\text{s}^{-1}$	Li-ion diffusion coefficient in electrolyte	$2.6\cdot 10^{-11}$	$[2.6\cdot 10^{-12}, 2.6\cdot 10^{-10}]$	(17b)
5	$D_{s,n}$	$\text{m}^2\cdot\text{s}^{-1}$	Li-ion diffusion coefficient in negative electrode	$2\cdot 10^{-14}$	$[2\cdot 10^{-18}, 2\cdot 10^{-10}]$	(17b)
6	$D_{s,p}$	$\text{m}^2\cdot\text{s}^{-1}$	Li-ion diffusion coefficient in positive electrode	$3.7\cdot 10^{-16}$	$[1.7\cdot 10^{-20}, 8\cdot 10^{-12}]$	(17b)
7	t_+		Transference number	0.35	[0.3, 0.4]	(17a)
8	R_e	μm	Radius of electrode material particle	1	[0.1, 10]	(17b)
9	α_n		Charge transfer coefficients in negative electrode	0.5	[0.3, 0.7]	(17a)
10	α_p		Charge transfer coefficients in positive electrode	0.5	[0.3, 0.7]	(17a)
11	$k_{0,n}$	$\text{A}\cdot\text{m}^{5/2}\cdot\text{mol}^{-3/2}$	Kinetic constant in negative electrode	$1.38\cdot 10^{-5.5}$	$[1.38\cdot 10^{-7}, 1.38\cdot 10^{-4}]$	(17b)
12	$k_{0,p}$	$\text{A}\cdot\text{m}^{5/2}\cdot\text{mol}^{-3/2}$	Kinetic constant in positive electrode	$0.64\cdot 10^{-5.5}$	$[0.64\cdot 10^{-7}, 0.64\cdot 10^{-4}]$	(17b)
13	σ_n	$\text{S}\cdot\text{m}^{-1}$	Electrical conductivity in negative electrode	1000	[10, 10^5]	(17b)
14	σ_p	$\text{S}\cdot\text{m}^{-1}$	Electrical conductivity in positive electrode	0.003	$[3\cdot 10^{-7}, 30]$	(17b)
15	$C_{e,0}$	$\text{mol}\cdot\text{m}^{-3}$	Initial electrolyte concentration	$1.2\cdot 10^3$	$[10^3, 1.5\cdot 10^3]$	(17b)
16	R_f	$\Omega\cdot\text{m}^2$	Contact resistance	$2\cdot 10^{-3}$	$[2\cdot 10^{-4}, 2\cdot 10^{-2}]$	(17b)

groups of parameters will be described, and the ranges and nominal values of the parameters will be given.

3.1. Thermodynamic parameters

The thermodynamic parameters describe the system in equilibrium, when all concentration profiles and potentials are stable over the time and all net reaction currents are zero. For a battery, this means that the thermodynamic parameters are related to the equilibrium voltage and the battery's maximum capacity, since both of them are obtained when the applied current is zero. While the equilibrium potential is given by nonlinear equation that depends on the normalised concentrations, see (12), the reversible maximum capacities of

the negative and positive electrodes are given by

$$Q_n = A \delta_- \epsilon_{s,n} C_{s,n}^{\max} (y_{100\%} - y_{0\%}) F, \quad (16a)$$

$$Q_p = A \delta_+ \epsilon_{s,p} C_{s,p}^{\max} (x_{0\%} - x_{100\%}) F, \quad (16b)$$

where $x_{100\%}$, $y_{100\%}$, $x_{0\%}$ and $y_{0\%}$ are stoichiometry at 100% and 0% SOC respectively, in both electrodes. According to these equations, the thermodynamic parameters are estimated and listed in Table 1.

Generally, batteries are manufactured with the similar geometry and composition, while different capacities are obtained through altering the plate area A of batteries. Therefore, the values of the remaining thermodynamic parameters presented in Table 1 are adopted from [27]. The only parameter that is not directly taken from [27] is plate area A . The real capacity of the battery used in the present work can be determined by specific estimation procedure, based on voltage extrapolation towards zero current, which will be described in Section 4. The value for plate area A is estimated by the proportional relationship between the capacity reported in [27] and that measured in the present work.

3.2. Kinetic parameters

The kinetic parameters are determined by the rate of charge transfer reactions and the speed of charge/mass transport by migration and diffusion. Furthermore, the voltage drop, caused by current flow in the current collectors is included in kinetic parameters. A summary of the kinetic parameters in the DFN model is given in the Table 1.

The range of every kinetic parameter presented in Table 1 is obtained by gathering different values for every parameter from the literature [9, 10, 17, 18, 19, 20, 28, 27, 29, 30, 31, 32, 33, 34], and setting the minimum and maximum value as the boundary of each kinetic parameter. Within the range, every parameter can be expressed on a linear or a logarithmic scale, i.e.,

$$p_i = \beta \underline{p}_i + (1 - \beta) \overline{p}_i, \quad (17a)$$

or

$$\log p_i = \beta \log \underline{p}_i + (1 - \beta) \log \overline{p}_i, \quad (17b)$$

1
2
3
4
5
6
7
8
9 where $\beta \in [0, 1]$, $p_i \in \mathbf{p}$ denotes every kinetic parameter, \underline{p}_i and \overline{p}_i represent
10 minimum and maximum value of the parameter, respectively. For the parame-
11 ters whose range is in the same order of magnitude, (17a) is used, while (17b) is
12 used to express the parameters whose range differ in orders of magnitude. This
13 is shown in the last column in Table 1. The nominal values for each parameter
14 are calculated by substituting $\beta = 0.5$ into either (17a) or (17b).
15
16
17
18
19

20 **4. Thermodynamic modelling**

21
22 The output voltage of a Li-ion battery depends strongly on the equilibrium
23 potentials of cathode and anode, which, in turn, depend on temperature and
24 amount of lithium stored in each electrode. Therefore, the equilibrium potential
25 functions of the cell have to be estimated in accordance with measured data.
26 As discussed in Section 3, the thermodynamic parameters are related to the
27 equilibrium potentials of the battery. Hence, the equilibrium potential func-
28 tions for both electrodes will be determined based on the estimated values of
29 thermodynamic parameters.
30
31
32
33
34

35 The methodology proposed in this paper for determining the equilibrium po-
36 tentials for both electrodes is as follows. First, an equilibrium voltage (EMF) of
37 the complete battery is estimated, which also yields the maximal capacity of the
38 battery. The method to estimate the EMF is described in [35]. Subsequently, the
39 thermodynamic parameter A is estimated using the available maximal capacity.
40 Finally, the function describing the negative electrode potential U_n is derived
41 from [27] and the function describing the positive potential U_p is determined on
42 the basis of total EMF and the thermodynamic parameters.
43
44
45
46
47

48 *4.1. EMF (equilibrium voltage) and capacity of the cell*

49
50 To estimate the equilibrium voltage, or EMF voltage, the battery is dis-
51 charged several times at a constant current at different C-rates, where dis-
52 charging is terminated at 2.7 V. The following C-rates has been employed for
53 discharging: 0.1, 0.2, 0.3, 0.5, 0.75, 1.00 and 1.25 C-rate. The results of these
54
55
56
57
58

Table 2: Estimated coefficients in positive and negative electrode potential functions

	$\gamma_{k,0}$	$\gamma_{k,1}$	$\gamma_{k,2}$	$\gamma_{k,3}$	$\gamma_{k,4}$	$\gamma_{k,5}$	$\gamma_{k,6}$	$\gamma_{k,7}$	$\gamma_{k,8}$	$\gamma_{k,9}$
$U_p (k = p)$	$-2.49 \cdot 10^3$	14.56	$-1.86 \cdot 10^2$	$8.14 \cdot 10^2$	$-2.56 \cdot 10^3$	$4.63 \cdot 10^3$	$-4.51 \cdot 10^3$	$1.90 \cdot 10^3$	$2.49 \cdot 10^3$	-0.052
$U_n (k = n)$	$-8.63 \cdot 10^{-4}$	0	8.00	-12.58	5.07	$2.18 \cdot 10^{-5}$	0.019	15	-5.19	-2.43

measurements are used to determine the EMF based on the voltage extrapolation towards zero current [35, 36]. Fig. 2 shows the measured discharge curves as functions of the amount of extracted charge Q_{out} (solid colored lines), together with the extrapolated equilibrium voltage curve (dashed black line).

The capacity of the battery is the maximal extracted charge $Q_{\text{out}}^{\text{max}}$. From the extrapolated EMF curve in Fig. 2, it can be seen that the capacity $Q_{\text{out}}^{\text{max}} = 12.7$ Ah. Thus, the plate area A is calculated as 1.84 m^2 according to the proportional relationship $Q_{\text{out}}^{\text{max}}/Q_1 = A/A_1$, where Q_1 and A_1 are the capacity and plate area of battery used in [27].

4.2. Positive electrode equilibrium potential function

As mentioned above, the function describing the equilibrium potential of the negative electrode U_n is taken from [27], while the function describing the equilibrium potential of the positive electrode U_p is computed using the equilibrium voltage U_{bat} . Namely, it holds that

$$U_{\text{bat}} = U_p - U_n, \quad (18)$$

where U_{bat} is the equilibrium voltage. The rationale behind this approach is based on the fact that the potential of the negative electrode contributes much less to total battery voltage than the potential of the positive electrode (see also Fig. 3). Moreover, much of the variation in equilibrium potentials of various cells types is due to differences in cathode chemistries, while there is much less variation in composition of graphite anodes, which makes their equilibrium potential almost standard. By that reason, an equilibrium voltage of anode U_n is taken from [27].

After the total battery EMF U_{bat} has been estimated by extrapolation towards zero current, and the negative electrode equilibrium potential is assumed

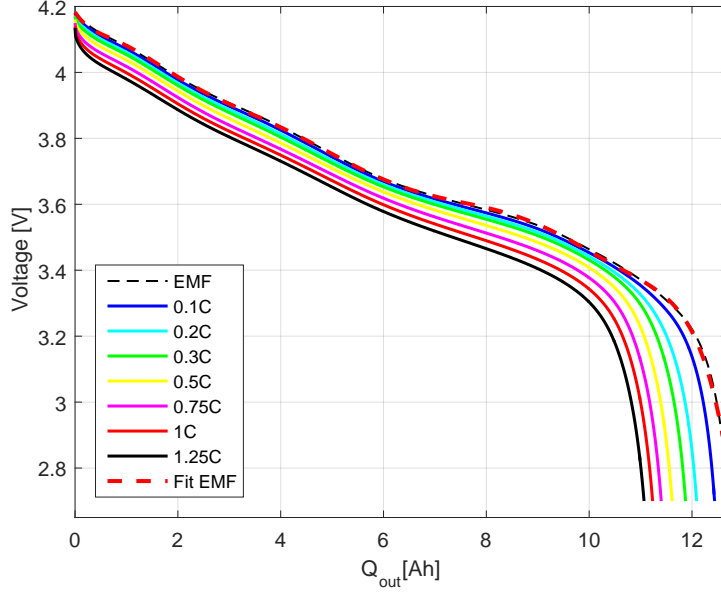


Figure 2: Set of discharge curves (0.1, 0.2, 0.3, 0.5, 0.75, 1.00) together with estimated U_{bat} and fitting result according to (19b).

to be given by (see [27])

$$U_n(y) = \sum_{i=0}^5 \gamma_{n,i} y^{\frac{i-2}{2}} + \gamma_{n,6} \exp(\gamma_{n,7} y) + \gamma_{n,8} \exp(\gamma_{n,9} y), \quad (19a)$$

the positive electrode equilibrium potential U_p can be computed using (18), which is then captured by the following expression:

$$U_p(x) = \sum_{i=0}^7 \gamma_{p,i} \left(\frac{x-x_{0\%}}{x_{100\%}-x_{0\%}} \right)^i + \gamma_{p,8} \exp\left(\gamma_{p,9} \left(\frac{x-x_{0\%}}{x_{100\%}-x_{0\%}} \right)^{10}\right), \quad (19b)$$

where $\gamma_{k,i}$, $i \in \{1, \dots, 9\}$, $k \in \{n, p\}$, are coefficients parameterizing these functions. Coefficients $\gamma_{p,i}$ are estimated by fitting the experimental data, while γ_i in U_n are obtained from [27]. All coefficients are listed in Table 2.

The dashed red line in Fig. 2 is the fitted result of total equilibrium (EMF) voltage, and Fig. 3 displays the resulting equilibrium potentials in the negative and positive electrodes, as functions of SoC. The dashed red line in Fig. 3 is the total EMF.

1
2
3
4
5
6
7
8
9
10
11
12
13
14
15
16
17
18
19
20
21
22
23
24
25
26
27
28
29
30
31
32
33
34
35
36
37
38
39
40
41
42
43
44
45
46
47
48
49
50
51
52
53
54
55
56
57
58
59
60
61
62
63
64
65

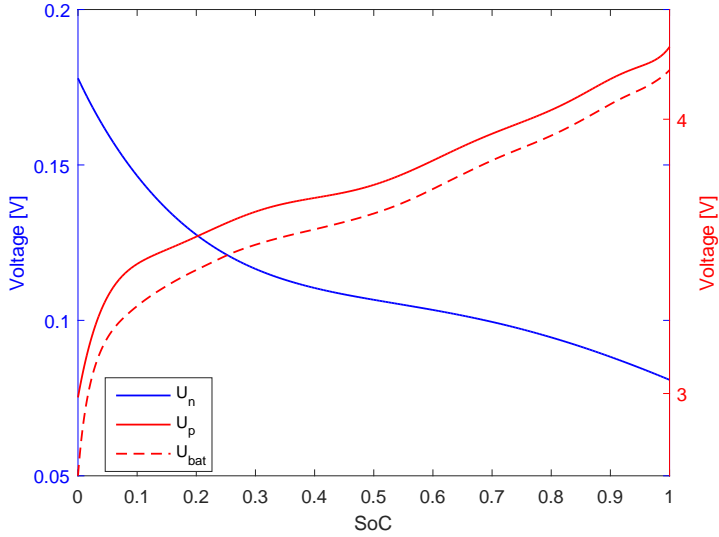


Figure 3: Equilibrium potentials in the negative electrode (solid blue line), and positive electrode (solid red line) and total EMF (dashed red line).

5. Kinetics modelling

After determining the thermodynamic parameters, the kinetic parameters have to be estimated. Identifying a large number of kinetic parameters from measurements leads to the question: which model properties can be estimated reliably from the available measurement data? To answer this question, the sensitivity of the battery voltage with respect to changes in the parameters can be investigated. If only some of the parameters are sensitive, then it is possible to reduce the complexity of the parameter estimation procedure and avoid large uncertainties in estimates, because only the sensitive parameters can be reliably estimated. Since the parameter sensitivity of the battery voltage depends on the choice of the current drawn from the battery, this current input design is an imperative premise of the followed sensitivity analysis and estimation.

5.1. Input design

An essential preparation for the sensitivity analysis and the parameter estimation is the design of a suitable input. The objective of input design is to

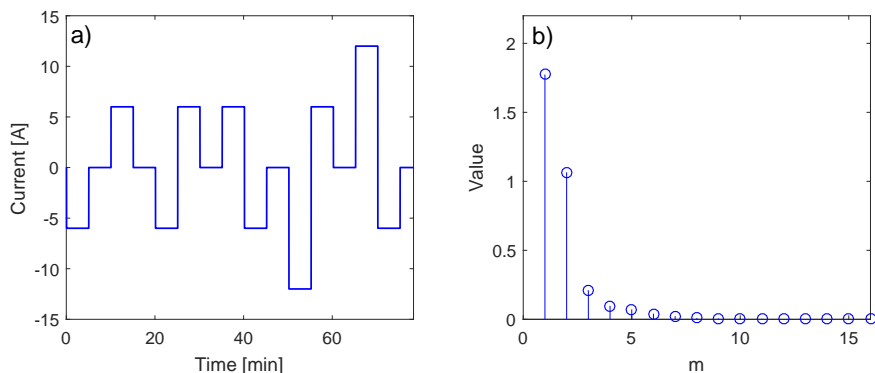


Figure 4: (a) designed input of the model, (b) magnitude of diagonal entries in matrix R.

generate informative data while experimentation effort is reduced. As the input of the model, the cell current has to excite the battery at various C-rates in order to cover different charging or discharging conditions. The design of input current is based on the following considerations:

- *Both charging and discharging:* The output voltage may reveal different dynamics when charging and discharging the battery since the response of the DFN model might not be symmetric.
- *Different C-rates:* The voltage response of the DFN model might depend nonlinearly on magnitude of the exciting current.
- *Relaxation:* In order to capture the voltage relaxation behavior of the cell, the (dis-)charging periods should be followed by zero current periods.

The input current designed according to the conditions above is shown in Fig. 4a. The excitation signal is composed of several periods, and different constant currents are applied in each period. The designed input $\mathbf{I}_{\text{app}}(t)$ includes charge and discharge pulses at 1C-rate and 0.5 C-rate, each pulse is followed by relaxation phase. The duration of each pulse and relaxation phase is 5 min, which is enough to capture the dynamics of the battery when current flows and during relaxation period.

1
2
3
4
5
6
7
8
9
10
11
12
13
14
15
16
17
18
19
20
21
22
23
24
25
26
27
28
29
30
31
32
33
34
35
36
37
38
39
40
41
42
43
44
45
46
47
48
49
50
51
52
53
54
55
56
57
58
59
60
61
62
63
64
65

5.2. Sensitivity analysis

The idea of estimating only a subset of the parameter set in the DFN model has been proposed before in [18, 20, 33, 34]. In particular, all the aforementioned papers propose to estimate some of the parameters, see Table 3, while keeping the others at some nominal value. It can be observed from Table 3 that no consensus exist on which parameter should be estimated. Moreover, a systematic approach for selecting which parameters can be reliably estimated does not seem to be present in these papers. In this paper, such a systematic approach is developed in the form of a parameter sensitivity analysis. The parameter sensitivity analysis determines how sensitive is the output of the model with respect to variation in values of parameters. Since the output of the DFN model depends nonlinearly on the parameters, this is a local analysis. Besides presenting a formal mathematical model, the method is illustrated numerically.

5.2.1. Parameter ranking by QR factorization

In this paper, the sensitive analysis is done using a QR factorization with column permutation [22] of a to-be-defined sensitivity matrix. To define this sensitivity matrix, let us write the predicted voltage output of the DFN model using the following nonlinear function:

$$\hat{\mathbf{V}} = h(\mathbf{I}_{app}, \mathbf{p}; \mathbf{C}_0, \phi_0), \quad (20)$$

where $\hat{\mathbf{V}} = [\hat{V}(t_1), \hat{V}(t_2), \dots, \hat{V}(t_N)]^T$, is a prediction of output voltage measurements of the battery stacked over time, and $h(\mathbf{I}_{app}, \mathbf{p}; \mathbf{C}_0, \phi_0)$ represents the solution to the DFN governing equations (15),

Table 3: Estimated parameters from various sources

Literature	Estimated Parameters
[18]	$\varepsilon_{e,sep}, t_+, \sigma_n, C_{e,0}$
[20]	$D_{s,p}, k_{0,n}, k_{0,p}, x_{100\%}, x_{0\%}, y_{100\%}, y_{0\%}$
[34]	$C_{s,n}^{max}, C_{s,p}^{max}, D_{s,n}, D_{s,p}, a_{s,n}, a_{s,p}, k_0$
[33]	$D_{s,n}, D_{s,p}, D_e, k_{0,n}, k_{0,p}$

where $\mathbf{I}_{\text{app}} = [I_{\text{app}}(t_1), I_{\text{app}}(t_2), \dots, I_{\text{app}}(t_N)]^T$, is the input current stacked over time. Finally, $\mathbf{p} = [p_1, p_2, \dots, p_m]^T \in \mathbf{P}$ is the parameter vector which contains all kinetic parameters and \mathbf{C}_0, ϕ_0 are the initial state vectors of concentrations and potentials.

Making a first-order Taylor expansion of the output of the model $\hat{\mathbf{V}}$ around its nominal parameters $\hat{\mathbf{p}}$ leads to

$$\hat{\mathbf{V}}(\mathbf{p}) = \hat{\mathbf{V}}(\hat{\mathbf{p}}) + \left. \frac{\partial \hat{\mathbf{V}}}{\partial \mathbf{p}} \right|_{\hat{\mathbf{p}}} (\mathbf{p} - \hat{\mathbf{p}}), \quad (21)$$

where the sensitivity matrix $\mathbf{S} = \left. \frac{\partial \hat{\mathbf{V}}}{\partial \mathbf{p}} \right|_{\hat{\mathbf{p}}}$ for the model output $\hat{\mathbf{V}}$ with respect to the kinetic parameters \mathbf{p} is given by the N by m matrix

$$\mathbf{S}(\mathbf{p}, \mathbf{t}) = \begin{bmatrix} s_1(\mathbf{p}, t_1) & s_2(\mathbf{p}, t_1) & \cdots & s_m(\mathbf{p}, t_1) \\ s_1(\mathbf{p}, t_2) & s_2(\mathbf{p}, t_2) & \cdots & s_m(\mathbf{p}, t_2) \\ \vdots & \vdots & \ddots & \vdots \\ s_1(\mathbf{p}, t_N) & s_2(\mathbf{p}, t_N) & \cdots & s_m(\mathbf{p}, t_N) \end{bmatrix}, \quad (22)$$

where N is a number of measurements, which is equal to the length of designed input, and $m = 16$, is the number of kinetic parameters. $s_j(\mathbf{p}, t_i) = \frac{\partial \hat{V}(t_i)}{\partial p_j}$ denotes the sensitivity of output $V(t_i)$ to parameter p_j , approximated using a finite-difference method. The output $\hat{\mathbf{V}}$ is obtained by supplying the designed input $\mathbf{I}_{\text{app}}(t_i)$ (cf. Fig. 4) to the model, while being at 50 % SoC and given certain nominal parameter value $\hat{\mathbf{p}} = [\hat{p}_1, \hat{p}_2, \dots, \hat{p}_m]$ (obtained by substituting $\beta = 0.5$ in (17a) or (17b)).

Each column of sensitivity matrix \mathbf{S} expresses the output sensitivity to every kinetic parameter. The norm of each column indicates the size of sensitivity while the linear dependence between two columns indicates the degree of similar effect on the output if changing these parameters. To allow comparing different parameters that have different orders of magnitude, the sensitivity matrix is normalized by multiplying with $\mathbf{\Gamma}_0$:

$$\mathbf{S}(\mathbf{p}, \mathbf{t})_{\text{norm}} = \mathbf{S}(\mathbf{p}, \mathbf{t})\mathbf{\Gamma}_0, \quad (23)$$

where $\mathbf{\Gamma}_0 = \text{diag}(\hat{p}_1, \hat{p}_2, \dots, \hat{p}_m)$ represents the diagonal matrix of nominal parameter values.

1
2
3
4
5
6
7
8
9 A QR factorization with column pivoting is a method that determines an
10 orthogonal matrix \mathbf{Q} , an upper triangular matrix \mathbf{R} , with a decreasing magni-
11 tude of diagonal entries $|r_{11}| \geq |r_{22}| \geq \dots \geq |r_{mm}|$, and a permutation matrix
12 $\mathbf{\Pi}$, so that
13

$$14 \quad \mathbf{S}_{\text{norm}} \mathbf{\Pi} = \mathbf{QR}. \quad (24)$$

15
16
17 The permutation matrix $\mathbf{\Pi}$ determines a new order of columns for matrix \mathbf{S}_{norm}
18 so that the most sensitive parameters appear in the first entries of the parameter
19 vector \mathbf{p} . The new ordering of parameters from most sensitive to least sensitive
20 can be computed using
21

$$22 \quad \begin{bmatrix} 1 & 2 & \dots & m \end{bmatrix} \mathbf{\Pi}, \quad (25)$$

23 where $[1 \ 2 \ \dots \ m]$ is the initial order of parameters. A detailed explanation of
24 sensitivity analysis based on the QR decomposition is given in [37] and some
25 examples employing this method are given in [22, 38].
26

27
28 When applying the QR factorization to the sensitivity matrix obtained by
29 applying the current input \mathbf{I}_{app} (cf. Fig. 4a) at 50% SOC, the order of param-
30 eters ranking from the most sensitive to the least is given by
31

$$32 \quad \begin{bmatrix} 1 & 2 & \dots & 16 \end{bmatrix} \mathbf{\Pi} = \begin{bmatrix} 8 & 14 & 4 & 6 & 16 & \dots \end{bmatrix}. \quad (26)$$

33
34 To assess how many parameter are sufficiently sensitive, the diagonal entries in
35 \mathbf{R} are considered, which are shown in Fig. 4b. From this figure, it can be seen
36 that the first five values are much larger than the others. This means that five
37 parameters are sufficiently sensitive. The extremely small values correspond to
38 the directions in the parameter space in which varying the parameters has very
39 limited influence on the output, leading to an unreliable parameter estimation,
40 and these parameters will be kept at their nominal values. Hence, only the
41 parameters corresponding to the first five indices will be estimated, which are
42 $[8, 14, 4, 6, 16]$. By looking up the number in the kinetic parameters in Table 1,
43 this corresponds to the parameters $\mathbf{p}_s = [R_s, \sigma_p, D_e, D_{s,p}, R_f]^T$, which are listed
44 in Table 4, ranking from the most sensitive parameter to the least sensitive one.
45 It should be noted that the conclusions presented here are based on the current
46
47
48
49
50
51
52
53
54
55
56
57
58
59
60
61
62
63
64
65

Table 4: Parameters ranking in the DFN model using QR

Selected Parameters		
Rank	Parameter	Description
1	R_s	Radius of electrode material particle
2	σ_p	Solid phase electrical conductivity in positive electrode
3	D_e	Li-ion diffusion coefficient in electrolyte
4	$D_{s,p}$	Li-ion diffusion coefficient in positive electrode
5	R_f	Contact resistance

input \mathbf{I}_{app} given in Fig. 4a at 50% SOC. However, the analysis has been done at 20% (an almost empty battery) and 80% SOC (an almost full battery), and for other current inputs, and the conclusions on the sensitive parameters remained the same.

5.2.2. Numerical illustration

To illustrate that the method based on the QR factorization indeed properly captures the sufficiently sensitive parameters, a numerical illustration is given. To illustrate the sensitivity of the parameters, a perturbation is given to every nominal kinetic parameter to see whether these changes influences the model output.

Consider the battery at 50% SOC, apply $\mathbf{I}_{\text{app}}(t)$ as given in Fig. 4a to the model and substitute $\beta = 0.4$ in (17a) or (17b) to increase each parameter by the same extent based on its nominal value. The model output is compared with that derived by using nominal values $\hat{\mathbf{p}}$. The same is done for decreasing the parameters by replacing $\beta = 0.6$. It turns out that $R_s, \sigma_p, D_e, D_{s,p}$ and R_f are sensitive parameters since the variation in model output $\hat{\mathbf{V}}(t)$ is obvious when changing these parameters, which is reflected in the first five plots in Fig. 5. However, for the transference number t_+ , which is the first non-identifiable parameter (ranking sixth in sensitivity), the output of the model is non-sensitive to the deviation of t_+ from its nominal value, as the last plot in Fig. 5 shows.

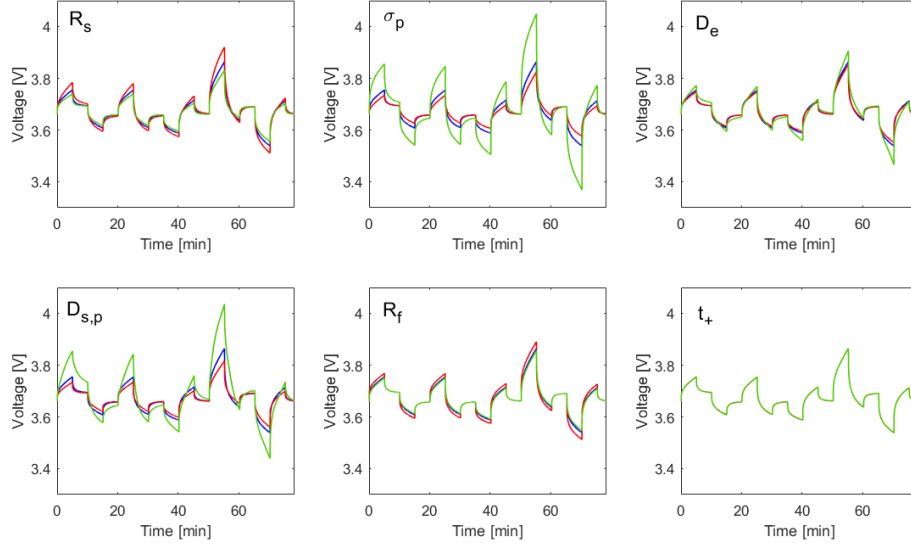


Figure 5: Comparison of model output by changing parameters. Blue lines are $\beta = 0.5$, red lines are $\beta = 0.4$ and green lines are $\beta = 0.6$.

5.3. Parameter estimation

After selecting parameters which can be properly estimated using the dynamic current input of Fig. 4a, the kinetic parameters are now estimated by minimizing the sum of the squared error between experimental voltage and predicted one, i.e.

$$\hat{\mathbf{p}}_s := \arg \min_{\mathbf{p}_s} \sum_{i=1}^N (V_{\text{exp}}(t_i) - \hat{V}(\mathbf{p}_s, t_i))^2 \quad (27)$$

where $V_{\text{exp}}(t_i)$ denotes the measurement of voltage, $\hat{V}(\mathbf{p}_s, t_i)$ is the predicted output voltage and \mathbf{p}_s is a vector of identifiable parameters.

In this paper, a nonlinear least-squares regression technique called the Levenberg-Marquardt method [24] is used to solve (27) and to obtain parameter estimates. The Levenberg-Marquardt algorithm is implemented in Matlab by the function *nonlsq* and it actually consists of a combination of two minimization methods: the gradient descent method and the Gauss-Newton method [24]. The update rule is given by

$$\hat{\mathbf{p}}_{s,\ell+1} = \hat{\mathbf{p}}_{s,\ell} + (\mathbf{J}_\ell^T \mathbf{J}_\ell + \lambda_\ell \mathbf{I})^{-1} \mathbf{J}_\ell^T \mathbf{f}_\ell, \quad (28)$$

Table 5: Estimated values of first five most sensitive parameters using Levenberg-Marquardt method

Parameter	Dimension	Initial value	Optimized value
R_s	μm	1	0.834
σ_p	$\text{S}\cdot\text{m}^{-1}$	$3 \cdot 10^{-3}$	$2 \cdot 10^{-3}$
D_e	$\text{m}^2\cdot\text{s}^{-1}$	$2.6 \cdot 10^{-11}$	$1.66 \cdot 10^{-11}$
$D_{s,p}$	$\text{m}^2\cdot\text{s}^{-1}$	$3.7 \cdot 10^{-16}$	$8.38 \cdot 10^{-16}$
R_f	$\Omega\cdot\text{m}^2$	$2 \cdot 10^{-3}$	$2.4 \cdot 10^{-3}$

where $\ell \in \mathbb{N}$ is the iteration index, $\lambda_\ell > 0$ is a well-chosen damping factor, $\mathbf{f}_\ell = \mathbf{V}_{\text{exp}} - \hat{\mathbf{V}}(\hat{\mathbf{p}}_{s,\ell})$, $\mathbf{V}_{\text{exp}} = [V_{\text{exp}}(t_1), \dots, V_{\text{exp}}(t_N)]^T$ and $\hat{\mathbf{V}}(\hat{\mathbf{p}}_{s,\ell}) = [\hat{V}(\hat{\mathbf{p}}_{s,\ell}, t_1), \dots, \hat{V}(\hat{\mathbf{p}}_{s,\ell}, t_N)]^T$. The matrix \mathbf{J}_ℓ is a Jacobian matrix of the partial derivatives of the output voltage $\hat{\mathbf{V}}(\mathbf{p}_s)$ with respect to all the parameters \mathbf{p}_s , and is evaluated in local parameter $\hat{\mathbf{p}}_{s,\ell}$ at each iteration, i.e., $\mathbf{J}_\ell = \left. \frac{\partial \hat{\mathbf{V}}(\mathbf{p}_s)}{\partial \mathbf{p}_s} \right|_{\hat{\mathbf{p}}_{s,\ell}}$.

Since different information will be obtained when starting (dis-)charging a nearly empty or a full battery, the experimental data \mathbf{V}_{exp} are collected by giving the designed input $\mathbf{I}_{\text{app}}(t)$ (Fig. 4a) to the battery at both 20% and 80% SoC. The initial sensitive parameter vector $\hat{\mathbf{p}}_{s,0}$ is chosen as the nominal values, as given by Table 1, and the final identifiable parameter estimates $\hat{\mathbf{p}}_s$ are obtained via an iterative procedure using (28) until it has converged and provides a solution to (27). The obtained parameter estimates are given in Table 5. The predicted and experimental voltages at different initial SoC (80% and 20%) after the parameter estimation procedure are shown Fig. 6b,c. The solid blue and red lines represent the measured voltage and output of the identified model, respectively. It can be observed that the optimized parameter estimates lead to a model prediction that agrees quite well with the measured voltages at both SoC.

1
2
3
4
5
6
7
8
9
10
11
12
13
14
15
16
17
18
19
20
21
22
23
24
25
26
27
28
29
30
31
32
33
34
35
36
37
38
39
40
41
42
43
44
45
46
47
48
49
50
51
52
53
54
55
56
57
58
59
60
61
62
63
64
65

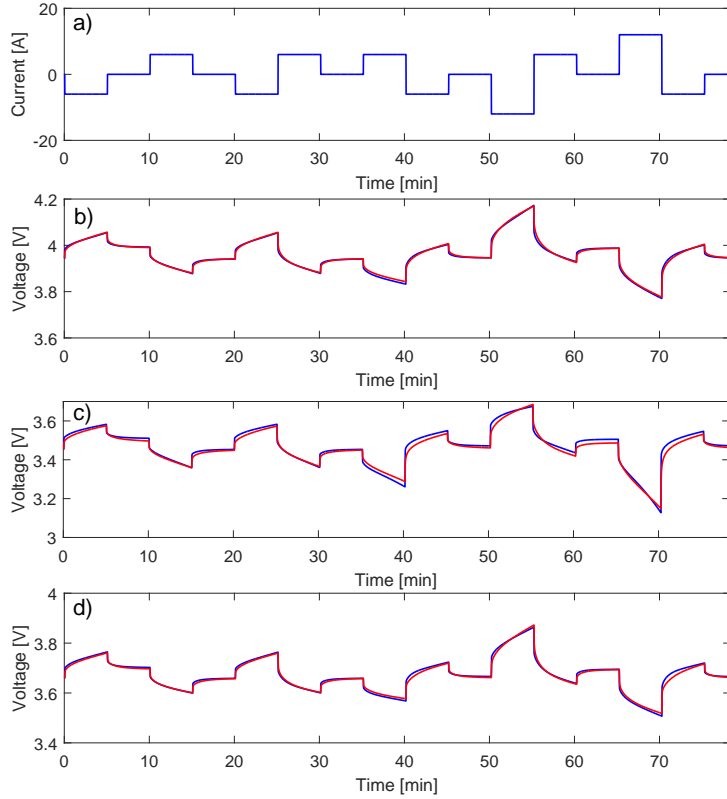


Figure 6: a) designed input current profile; battery measurement (blue) and battery model predictions (red) at: b) 80% SoC, estimation phase; c) 20% SoC, estimation phase; d) 50% SoC, validation phase.

6. Validation

In this section, the model with the optimised values of the parameters will be validated on different data sets. Constant currents and pulsed current profiles will be used in the model validation.

6.1. Static discharge experiments

The constant discharge reveals how the battery performs in the whole process from the full to the empty. Substitute the estimated parameters into the model and give the constant currents 12A, 6A and 1.2A, as inputs to the model, to discharge the battery at 1C-rate, 0.5C-rate and 0.1C-rate respectively. Fig. 7

1
2
3
4
5
6
7
8
9
10
11
12
13
14
15
16
17
18
19
20
21
22
23
24
25
26
27
28
29
30
31
32
33
34
35
36
37
38
39
40
41
42
43
44
45
46
47
48
49
50
51
52
53
54
55
56
57
58
59
60
61
62
63
64
65

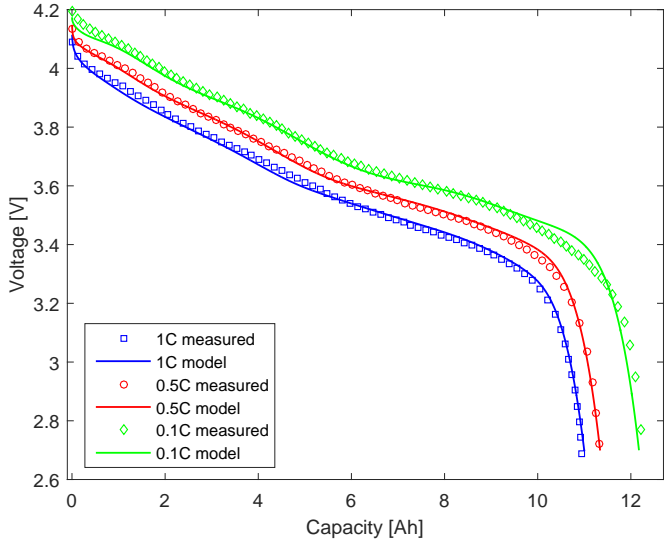


Figure 7: Battery measurements (symbols) versus battery model predictions (lines) during validation phase, under constant discharge current.

presents the comparison of the model predictions to the experimental data when discharging the battery in various C-rates. The solid colored lines represent measured data and the symbols stand for the predicted voltage of the model. It can be seen that the model output is in good agreement with the measured data in the static discharges.

6.2. Pulses experiments

Besides the constant currents, the validation is also done on pulsed (dis-)charge inputs to assure that the estimated model is durable to capture the dynamics of battery. In Section 5, the experimental data sets at 20% and 80% SoC are utilized for estimation, so it is sensible to validate on the measured voltage at 50% SoC (the middle of the entire range of SoC). The input profile is the same as that used in parameter estimation, but the initial SoC has changed to 50%. Fig. 6d shows the simulation result compared to the measured data when starting at 50% SoC. Additionally, another input with shorter pulses and longer relaxation periods is used for validation. The input is characterized by

Table 6: RMSE between predictions and various experimental data sets

Input [A]	RMSE [mV]
Fig. 6b	5.6
Fig. 6c	15.5
Fig. 6d	7.2
Fig. 8b	5.9

several pulses last 2 min, each is followed by 10 min relaxation period. Fig. 8 displays the validation result on this input profile.

From Fig. 6d and Fig. 8, it can be observed that the prediction of voltage for the identified model agrees with the experimental ones well. The Root Mean Square Error (RMSE) between the predictions and various experimental data sets is calculated and reported in Table 6. The error at 80% SoC is the smallest, RMSE is 5.6 mV, while RMSE at 20% SoC is the largest, 15.5 mV. Regardless of what initial SoC the battery start at and what durations of the pulses and relaxation periods are in the input, RMSE values are small, which indicates the identified battery model is in good agreement with real behavior of the battery in pulses (dis-)charge.

7. Conclusions

The Doyle-Fuller-Newman (DFN) model is one of the most popular models in describing the behavior of the Li-ion battery, and contains a large number of parameters. It is important to estimate parameters in the DFN model to obtain an accurate model for simulation or solving control-oriented problems. In this paper, a computationally feasible two-step estimation approach is developed in which the original set of parameters is split into two. The first set contains thermodynamically determined parameters, which have been estimated on the set of static discharge curves by extrapolating towards zero current. The second set contains kinetic parameters, which have been estimated using a designed highly-dynamic pulse (dis-)charge current. A sensitivity analysis based on QR

1
2
3
4
5
6
7
8
9
10
11
12
13
14
15
16
17
18
19
20
21
22
23
24
25
26
27
28
29
30
31
32
33
34
35
36
37
38
39
40
41
42
43
44
45
46
47
48
49
50
51
52
53
54
55
56
57
58
59
60
61
62
63
64
65

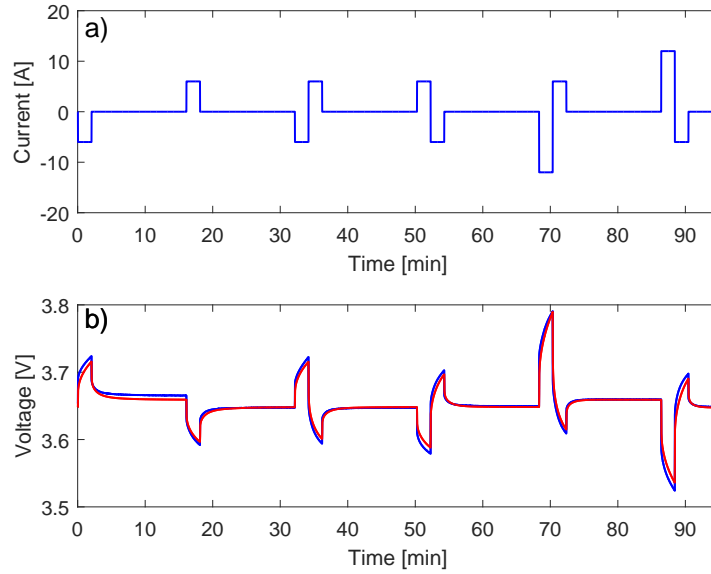


Figure 8: a) validation input current profile, b) battery voltage measurements (blue) and battery model predictions (red) under validation input current profile at 50% SoC.

factorization with column pivoting has been done to find out the most sensitive kinetic parameters. Estimating only the sufficiently sensitive parameters leads to a more reliable estimation result.

The sufficiently sensitive parameters have been estimated through minimizing the sum of square error between experimental data and predicted voltage using the Levenberg-Marquardt method, which was selected for the parameter estimation due to its fast convergence. The result was illustrated by comparing the model outputs with the battery measurements, and a quite well fit was achieved. Finally, the estimated model has been validated on several specifically designed validation data sets. Validation results reveal an error in output voltage of less than 16 mV RMSE of magnitude. Therefore, a good performance of the identified model in predicting the experiment results is demonstrated.

1
2
3
4
5
6
7
8
9 **8. Acknowledgements**

10
11 This work has received financial support from the Horizon 2020 program of
12 the European Union under the grant ‘Integrated Components for Complexity
13 Control in affordable electrified cars (3Ccar-662192)’ and under the grant ‘Elec-
14 tric Vehicle Enhanced Range, Lifetime And Safety Through INGenious battery
15 management (EVERLASTING-713771)’. The authors would also like to thank
16 Prof. Peter H.L. Notten from Eindhoven University of Technology for his fruitful
17 discussions.
18
19
20
21
22

23
24 **References**

- 25
26 [1] C. Fellner, J. Newman, High-power batteries for use in hybrid vehicles,
27 Journal of Power Sources 85 (2) (2000) 229–236.
28
29 [2] S. B. Peterson, J. Whitacre, J. Apt, The economics of using plug-in hybrid
30 electric vehicle battery packs for grid storage, Journal of Power Sources
31 195 (8) (2010) 2377–2384.
32
33 [3] G. L. Plett, Extended kalman filtering for battery management systems
34 of lipb-based hev battery packs: Part 3. state and parameter estimation,
35 Journal of Power sources 134 (2) (2004) 277–292.
36
37 [4] Y. Xing, E. W. Ma, K. L. Tsui, M. Pecht, Battery management systems in
38 electric and hybrid vehicles, Energies 4 (11) (2011) 1840–1857.
39
40 [5] A. T. Stamps, C. E. Holland, R. E. White, E. P. Gatzke, Analysis of
41 capacity fade in a lithium ion battery, Journal of Power Sources 150 (2005)
42 229–239.
43
44 [6] A. Barré, B. Deguilhem, S. Grolleau, M. Gérard, F. Suard, D. Riu, A review
45 on lithium-ion battery ageing mechanisms and estimations for automotive
46 applications, Journal of Power Sources 241 (2013) 680–689.
47
48
49
50
51
52
53
54
55
56
57
58

- 1
2
3
4
5
6
7
8
9 [7] L. Lu, X. Han, J. Li, J. Hua, M. Ouyang, A review on the key issues
10 for lithium-ion battery management in electric vehicles, *Journal of power*
11 *sources* 226 (2013) 272–288.
12
13
14 [8] B. Y. Liaw, G. Nagasubramanian, R. G. Jungst, D. H. Doughty, Modeling
15 of lithium ion cells a simple equivalent-circuit model approach, *Solid state*
16 *ionics* 175 (1) (2004) 835–839.
17
18
19 [9] M. Doyle, T. F. Fuller, J. Newman, Modeling of galvanostatic charge and
20 discharge of the lithium/polymer/insertion cell, *Journal of the Electro-*
21 *chemical Society* 140 (6) (1993) 1526–1533.
22
23
24 [10] T. F. Fuller, M. Doyle, J. Newman, Simulation and optimization of the dual
25 lithium ion insertion cell, *Journal of the Electrochemical Society* 141 (1)
26 (1994) 1–10.
27
28
29 [11] Y. Hu, S. Yurkovich, Y. Guezennec, B. Yurkovich, A technique for dy-
30 namic battery model identification in automotive applications using linear
31 parameter varying structures, *Control Engineering Practice* 17 (10) (2009)
32 1190–1201.
33
34
35 [12] M. Sitterly, L. Y. Wang, G. G. Yin, C. Wang, Enhanced identification of
36 battery models for real-time battery management, *IEEE Transactions on*
37 *Sustainable Energy* 2 (3) (2011) 300–308.
38
39
40 [13] X. Tang, X. Mao, J. Lin, B. Koch, Li-ion battery parameter estimation
41 for state of charge, in: *American Control Conference (ACC)*, 2011, IEEE,
42 2011, pp. 941–946.
43
44
45 [14] C. Zhang, J. Liu, S. Sharkh, C. Zhang, Identification of dynamic model
46 parameters for lithium-ion batteries used in hybrid electric vehicles, *High*
47 *Technology Letters* 16 (1) (2010) 6–12.
48
49
50 [15] H. He, R. Xiong, J. Fan, Evaluation of lithium-ion battery equivalent cir-
51 cuit models for state of charge estimation by an experimental approach,
52 *Energies* 4 (4) (2011) 582–598.
53
54
55
56
57
58
59
60
61
62
63
64
65

- 1
2
3
4
5
6
7
8
9 [16] S. Santhanagopalan, Q. Guo, P. Ramadass, R. E. White, Review of models
10 for predicting the cycling performance of lithium ion batteries, *Journal of*
11 *Power Sources* 156 (2) (2006) 620–628.
12
13
14 [17] A. P. Schmidt, M. Bitzer, Á. W. Imre, L. Guzzella, Experiment-driven
15 electrochemical modeling and systematic parameterization for a lithium-
16 ion battery cell, *Journal of Power Sources* 195 (15) (2010) 5071–5080.
17
18
19 [18] R. Masoudi, T. Uchida, J. McPhee, Parameter estimation of an
20 electrochemistry-based lithium-ion battery model, *Journal of Power*
21 *Sources* 291 (2015) 215–224.
22
23
24 [19] A. Taghavipour, R. Masoudi, N. L. Azad, J. McPhee, High-fidelity mod-
25 eling of a power-split plug-in hybrid electric powertrain for control perfor-
26 mance evaluation, in: *ASME 2013 International Design Engineering Tech-*
27 *nical Conferences and Computers and Information in Engineering Confer-*
28 *ence*, American Society of Mechanical Engineers, 2013, pp. V001T01A008–
29 V001T01A008.
30
31
32 [20] S. Santhanagopalan, Q. Guo, R. E. White, Parameter estimation and model
33 discrimination for a lithium-ion cell, *Journal of the Electrochemical Society*
34 154 (3) (2007) A198–A206.
35
36
37 [21] J. C. Forman, S. J. Moura, J. L. Stein, H. K. Fathy, Genetic parameter
38 identification of the doyle-fuller-newman model from experimental cycling
39 of a lifepo 4 battery, in: *American Control Conference (ACC)*, 2011, IEEE,
40 2011, pp. 362–369.
41
42
43 [22] B. F. Lund, B. A. Foss, Parameter ranking by orthogonalization-applied to
44 nonlinear mechanistic models, *Automatica* 44 (1) (2008) 278–281.
45
46
47 [23] P. E. Gill, W. Murray, Algorithms for the solution of the nonlinear least-
48 squares problem, *SIAM Journal on Numerical Analysis* 15 (5) (1978) 977–
49 992.
50
51
52
53
54
55
56
57
58
59
60
61
62
63
64
65

- 1
2
3
4
5
6
7
8
9 [24] O. Nelles, *Nonlinear system identification: from classical approaches to*
10 *neural networks and fuzzy models*, Springer Science & Business Media,
11 2013.
12
13
14 [25] C. M. Doyle, *Design and simulation of lithium rechargeable batteries*,
15 Lawrence Berkeley National Laboratory.
16
17
18 [26] L. Xia, E. Najafi, H. J. Bergveld, M. C. F. Donkers, A fast simulation of an
19 electrochemistry-based lithium-ion battery model, submitted to 20th IFAC
20 World Congress.
21
22
23 [27] K. A. Smith, C. D. Rahn, C.-Y. Wang, Control oriented 1d electrochemical
24 model of lithium-ion battery, *Energy Conversion and management* 48 (9)
25 (2007) 2565–2578.
26
27
28 [28] S. Mazumder, J. Lu, Faster-than-real-time simulation of lithium ion bat-
29 teries with full spatial and temporal resolution, *International Journal of*
30 *Electrochemistry* 2013.
31
32
33 [29] M. Park, X. Zhang, M. Chung, G. B. Less, A. M. Sastry, A review of
34 conduction phenomena in li-ion batteries, *Journal of Power Sources* 195 (24)
35 (2010) 7904–7929.
36
37
38 [30] S. Santhanagopalan, Q. Zhang, K. Kumaresan, R. E. White, Parameter
39 estimation and life modeling of lithium-ion cells, *Journal of The Electro-*
40 *chemical Society* 155 (4) (2008) A345–A353.
41
42
43 [31] E. Martínez-Rosas, R. Vasquez-Medrano, A. Flores-Tlacuahuac, Modeling
44 and simulation of lithium-ion batteries, *Computers & Chemical Engineer-*
45 *ing* 35 (9) (2011) 1937–1948.
46
47
48 [32] T.-S. Dao, C. P. Vyasarayani, J. McPhee, Simplification and order reduc-
49 tion of lithium-ion battery model based on porous-electrode theory, *Journal*
50 *of Power Sources* 198 (2012) 329–337.
51
52
53
54
55
56
57
58
59
60
61
62
63
64
65

- 1
2
3
4
5
6
7
8
9 [33] V. Ramadesigan, K. Chen, N. A. Burns, V. Boovaragavan, R. D. Braatz,
10 V. R. Subramanian, Parameter estimation and capacity fade analysis of
11 lithium-ion batteries using reformulated models, *Journal of The Electro-*
12 *chemical Society* 158 (9) (2011) A1048–A1054.
13
14
15
16 [34] C. Speltino, D. Di Domenico, G. Fiengo, A. Stefanopoulou, Experimental
17 identification and validation of an electrochemical model of a lithium-ion
18 battery, in: *Control Conference (ECC), 2009 European, IEEE, 2009*, pp.
19 1053–1058.
20
21
22
23 [35] D. Danilov, R. Niessen, P. H. L. Notten, Modeling all-solid-state li-ion
24 batteries, *Journal of the Electrochemical Society* 158 (3) (2011) A215–
25 A222.
26
27
28 [36] V. Pop, H. J. Bergveld, D. Danilov, P. P. Regtien, P. H. L. Notten, *Bat-*
29 *ttery management systems: Accurate state-of-charge indication for battery-*
30 *powered applications*, Vol. 9, Springer Science & Business Media, 2008.
31
32
33
34 [37] G. Golub, Numerical methods for solving linear least squares problems,
35 *Numerische Mathematik* 7 (3) (1965) 206–216.
36
37
38 [38] M. Fink, A. Attarian, H. Tran, Subset selection for parameter estimation
39 in an hiv model, *PAMM* 7 (1) (2007) 1121501–1121502.
40
41
42
43
44
45
46
47
48
49
50
51
52
53
54
55
56
57
58
59
60
61
62
63
64
65